Identification of Tip-Leakage Vortex Wandering in Large-Eddy Simulation of ECL5/CATANA Transonic Fan Stage

Allan Beurville, Valentin Caries, Jérôme Boudet, Vincent Clair, Alexis Giauque

Proceedings of the 16th European Turbomachinery Conference (ETC16)
Turbomachinery, Fluid Dynamics and Thermodynamics,
March 24-28, 2025; Hannover, Germany

Identification of Tip-Leakage Vortex Wandering in Large-Eddy Simulation of ECL5/CATANA Transonic Fan Stage

A. Beurville*[1], V. Caries[1,2], J. Boudet[1], V. Clair[1], and A. Giauque[1]

[1]École Centrale de Lyon, CNRS, Universite Claude Bernard Lyon 1, INSA Lyon, LMFA, UMR5509, 69130, Ecully, France
[2]Safran Aircraft Engines, Moissy-Cramayel, France

Abstract

The tip-leakage flow in fan stages affects aerodynamic efficiency, stability and contributes to broadband noise. Its behavior is difficult to predict, especially in transonic configurations. This study focuses on the ECL5 fan/OGV stage, an open test case from École Centrale de Lyon. At nominal speed, the flow is transonic, with a relative Mach number at the inlet slightly above unity near the tip. A large-eddy simulation (LES) is performed on a periodic angular sector to simulate the unsteady flow phenomena. A first comparison with experimental measurements focuses on the validation of the LES. The analysis of the pressure fluctuation spectra reveals an unexpected low-frequency peak upstream of the rotor blades. A dynamic mode decomposition at the corresponding frequency shows an unsteadiness in the tip-leakage flow. Tracking the tip-leakage flow dynamically using conventional vortex identification methods such as Galilean invariants can be challenging, especially in complex flow conditions. A purely kinetic vortex tracking algorithm is developed and validated to determine the trajectory and size evolution of the tip-leakage vortex. In the mean flow, the vortex is detected up to two rotor chords downstream of the leading edge of the rotor blade. By using frequency-filtered fields from the unsteady simulation, vortex wandering is investigated. The interaction with the surrounding flow features is outlined.
Keywords: Large-Eddy Simulation, Tip-Leakage Vortex, Transonic Fan, Vortex Wandering, Vortex Tracking.

Nomenclature

Roman letters

$\dot{m}_{std}$	mass-flow rate (kg/s)
Π	total pressure ratio
P_0	total pressure (Pa)
T_0	total temperature (K)
y^+	dimensionless wall-normal distance

Greek letters

Γ_1, Γ_2	vortex tracking sensor
Ω	rotational speed (RPM)

Abbreviations

BPF	blade passing frequency
DMD	dynamic mode decomposition
LES	large eddy simulation
NSCBC	Navier-Stokes characteristic boundary conditions
NSV	non-synchronous vibrations
OGV	outlet guide vanes
PSD	power spectrum density
TLV	tip-leakage vortex
TTG	two-step Taylor Galerkin
UHBR	ultra high by-pass ration

1 Introduction

Modern design of turbofan jet engines tends to increase the radius of the fan blades in order to increase the by-pass ratio and the efficiency. Therefore, the flow can be transonic and the blades have to be designed to handle the transonic regime. Thin blades are prone to non-synchronous vibrations (NSV), leading to a reduction of the stability range of the fan-stage.

The tip-leakage vortex (TLV) is recognized as a main contributor to flow structures during NSV. The wandering [1] phenomenon of the TLV can be the precursor of NSV. Identifying unsteady phenomena such as wandering can be tedious using only low order models. This paper develops a vortex tracking algorithm to detect the unsteady TLV from large eddy simulations (LES).

The study focuses on simulations performed at the design point of the ECL5 fan/OGV stage [2–4].

In fluid dynamics, different criteria are usually used in order to detect vortices. In computational fluid dynamics, one can use Galilean invariants such as the Q-criterion [5], the Δ-criterion [6] or the λ_2-criterion [7]. Those methods are based on the velocity gradient tensor. The sign of those Galilean invariants is used to locate vortices. Vortex identification is performed by extracting an iso-surface of a given criterion [7]. However this approach seems limited by the the criterion value and remains qualitative. Depending on the flow, larger absolute values of the criterion lead to thin but very local structures, while smaller absolute values lead to larger structures. Another methodology to identify vortices was developed for particle image velocimetry by Graftieaux [8], due to the inaccessibility of velocity gradients. The Γ_2 criterion

has been shown to be noise resilient [9, 10], but remains qualitative, and formally limited to incompressible flows. The purpose of this paper is to extend the method developed by Graftieaux to a compressible flow, by coupling the Γ_2 criterion with Galilean invariants.

2 Study case – ECL5

This study focuses on the ECL5 fan/OGV stage, an open test case designed at École Centrale de Lyon [2–4]. The stage is made of 16 rotor blades and 31 stator vanes. This Ultra High By-pass Ratio (UHBR) fan/OGV stage is part of the European CATANA project and aims to openly provide design, simulations and experimental measurements to the community, in order to provide a multi-physical validation benchmark representative of near-future UHBR fan concepts. Several experimental campaigns were performed within the PHARE-2 test facility. The experimental campaigns comprised investigations of stable operating points and instability mechanisms such as NSV [11].

LES are performed on the ECL5 fan/OGV stage and the computational cost of the LES is reduced by computing a periodic angular sector of the fan/OGV stage. In order to preserve the angular extent for the rotor and the stator domains, the initial 31 vanes are adapted to 32 vanes. The fan stage performance is maintained by adjusting the chord length of the vanes [12] by a 31/32 factor.

The present work is performed at the design point of the ECL5 at nominal speed ($\Omega = 11\,000$ RPM). The corresponding inflow axial Mach number is 0.53 and the inlet relative Mach number at the fan blade tip is slightly above 1. The blade passage frequency is equal to 2933 Hz.

Simulations of the ECL5 fan stage are performed using AVBP, an explicit unstructured fully compressible LES solver developed by CERFACS [13–15]. For turbomachinery applications, the resolution is performed over two domains: a rotating domain containing one rotor blade and a static domain containing two stator vanes. A third order interpolation is performed at every time-step to couple the domains. The coupling is ensured by the MISCOG methodology [16, 17]. Computational performance is preserved using the CWIPI library (ONERA) [18].

The simulations are carried out using a third order Two-step Taylor Galerkin (TTGC) convection scheme [19]. Unresolved turbulent eddies are modelled using the SIGMA subgrid scale model [20]. Shockwaves are handled using the Cook and Cabot hyperviscosity model [21]. Non-reflecting Navier-Stokes characteristic boundary conditions (NSCBC) are used both at the inlet and at the outlet [22]. A wall function (linear law below $y^+ = 11.45$, log law otherwise) is used near the walls in order to limit the computational cost [23, 24]. Simulations are performed on a hybrid unstructured mesh. The mesh contains approximately 100 millions cells. The dimensionless wall-normal distance y^+ of the first prismatic layer is under 35 on the blade skin. The time step for the simulation is slightly above $\Delta t = 1.6 \cdot 10^{-8}$ s. The computational time is 200×10^3 CPUh for one rotation.

The validation of the LES-averaged results with the experimental campaign are highlighted in figures 1 and 2. The time-averaged LES results are obtained by using 33,000 snapshots per rotation for 5 full rotations of the rotor. Figure 1 places the performance of the ECL5 fan/OGV stage obtained by the periodic sector LES on the experimental characteristic curve. The experimental reference is represented with ● while the periodic LES is marked with ⊗. The LES lies correctly on the experimental characteristic curve. Figure 2 compares the radial profiles of total pressure ratio and total temperature ratio at the stator domain exit plane, two chords downstream of the vanes' trailing edge. Both quantities follow the same trend, and a good agreement is observed between the LES and the experiment. The only significant differences occur near the casing.

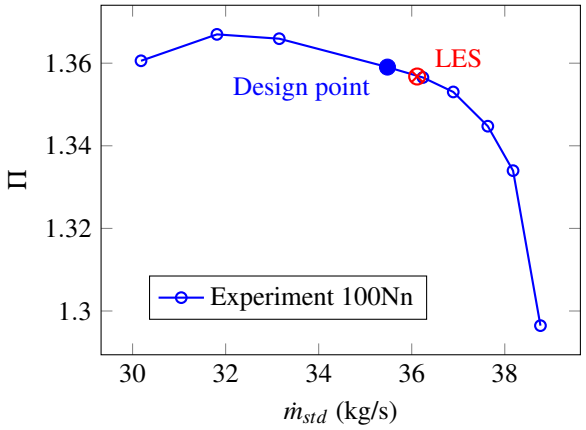

Figure 1: Comparison of the characteristics (mass-flow rate and total pressure ratio) of the periodic sector LES with the experimental measurements.

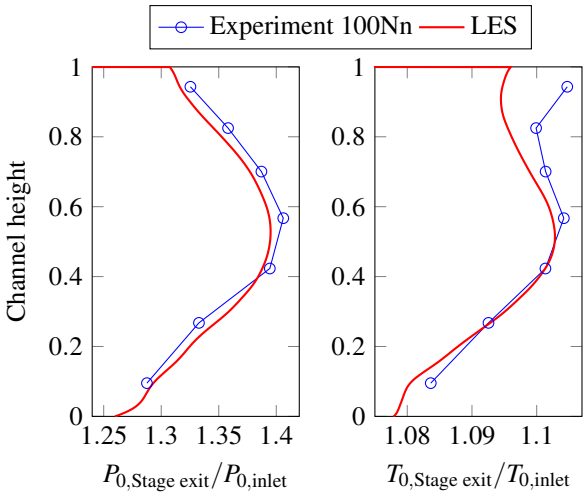

Figure 2: Comparison of the radial profiles of total pressure ratio and total temperature ratio in the stage domain exit plane. The stage domain exit plane is located two chords downstream of the trailing edge of the vanes.

Several blade-to-blade views are provided in figure 3. Figures 3a and 3c depict the average relative Mach number and the average Mach number at 80% of the span around the rotor and stator respectively. The sonic line is highlighted in white. The supersonic region extends up to 40% of the chord

on the suction side of the rotor blade. Figure 3b represents the average relative Mach number at 99% of the rotor span. The flow is entirely supersonic upstream of the rotor blade but transitions to a subsonic regime in the tip leakage flow.

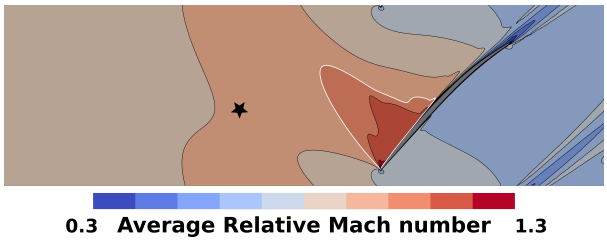

(a) Rotor 80% of span

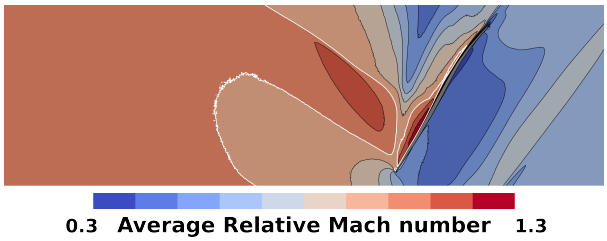

(b) Rotor 99% of span

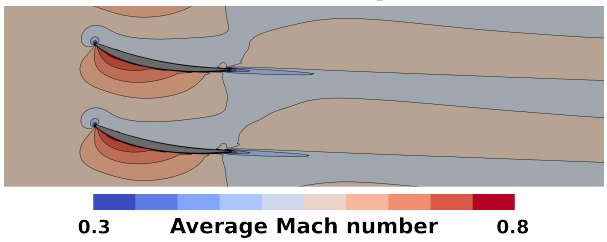

(c) Stator 80% of span

Figure 3: Average relative Mach number at different radial positions in the rotor domain (a, b) and the stator domain (c). A temporal signal is extracted from a stationary probe indicated by a star in figure (a).

The power spectral density of the pressure signal extracted from a probe located one chord upstream of the rotor blade (represented by a star in the figure 3a) is shown in figure 4. This probe is stationary in the absolute frame of reference. As expected, peaks appear at the blade passing frequency and its harmonics. However, another peak appears at low frequency, at about one fourth of the BPF, approximately at 750 Hz (highlighted in red in Figure 4).

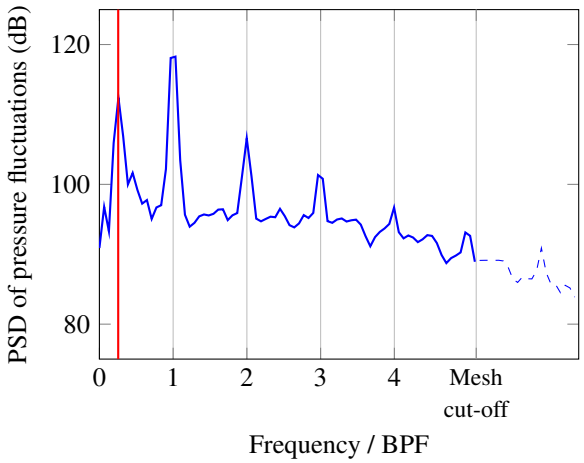

Figure 4: Power spectral density of the pressure fluctuations at the stationary probe one chord upstream the rotor blade at 80% of the span.

Therefore, one might want to look at the tip leakage flow in order to understand how the boundary layer on the casing, the supersonic region and the tip leakage vortex interact. However, extracting an iso-surface of a Galilean invariant is tedious in this case. Figure 5 provides iso-surface of the Q-criterion and λ_2-criterion for both the instantaneous and the average solution. For the mean flow, both iso-surfaces capture the shape of the TLV up to only 40% of the chord downstream of the leading edge. For the instantaneous flow, the tip leakage flow is complex and the identification of a specific structure is difficult.

In order to extract the tip leakage vortex from both the average and the instantaneous flow, a dedicated vortex tracking methodology is developed and used.

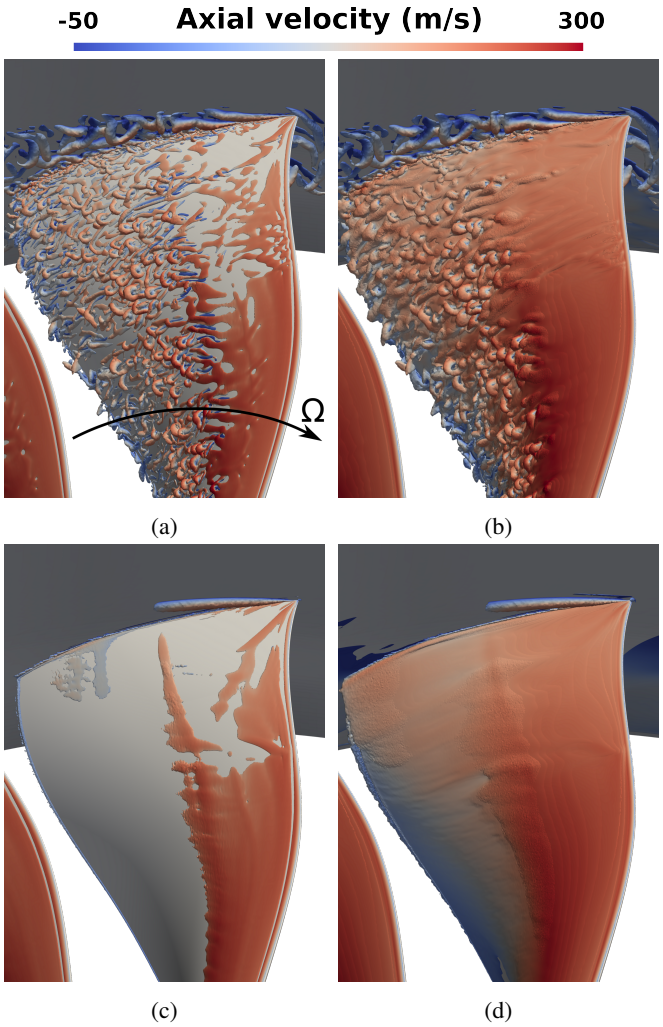

Figure 5: Iso-surfaces of Galilean invariants for both the instantaneous and mean flows. (a) and (c) are iso-surfaces of the Q-criterion for instantaneous and mean flows respectively. (b) and (d) are iso-surfaces of the λ_2-criterion for instantaneous and mean flows respectively.

3 Vortex Tracking Methodology

The vortex detection algorithm uses two scalar functions, Γ_1 and Γ_2, from Graftieaux et al. [8], to identify the vortex center and shape from velocity fields. As shown by Figure 6, for a given point P in the plane, the scalar functions are defined by:

$$\Gamma_i(P) = \frac{1}{S}\iint_{M\in S} \frac{(\mathbf{PM}\wedge\mathbf{U_i})\cdot\mathbf{n}}{\|\mathbf{PM}\|\cdot\|\mathbf{U_i}\|}\,\mathrm{d}S \tag{1}$$

$$\mathbf{U_i} = \begin{cases} \mathbf{U_M} & \text{for } i=1 \\ \mathbf{U_M}-\mathbf{U_P} & \text{for } i=2 \end{cases}$$

$$\mathbf{U_P} = \frac{1}{S}\iint_{N\in S} \mathbf{U_N}\,\mathrm{d}S$$

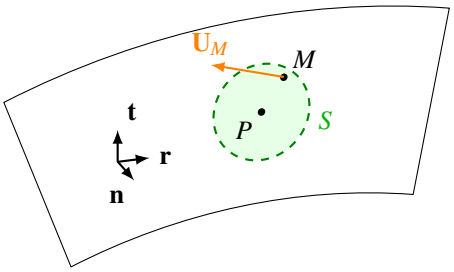

Figure 6: Calculation of Γ_1 and Γ_2 in a 2D plane.

Where S is a two-dimensional surface surrounding P, $\mathbf{U}_M$ is the velocity at the neighbor point M, and $(\mathbf{n},\mathbf{r},\mathbf{t})$ are the unit vectors in the reference frame of a plane.

The function Γ_1, which ranges from -1 to 1, is interpreted as the normalized angular momentum and is not Galilean invariant. The maximum of Γ_1 corresponds to the vortex center, and the sign indicates the direction of rotation. As shown by Graftieaux *et al.* [8], the evolution of Γ_1 with distance exhibits a narrow maximum, which is suitable for the precise identification of the vortex center. For practical identification, the maximum $|\Gamma_1|$ value must satisfy a threshold $|\Gamma_1| \geq 0.85$ to ensure an accurate detection.

The Γ_2 function evaluates the vortex core region. Γ_2 is Galilean invariant and depends on the local rotation rate and the eigenvalue of the strain rate for a sufficiently small integration surface S. The criterion $|\Gamma_2| > 2/\pi$ indicates a region dominated by rotational flows.

The integration of these quantities is performed numerically by summing the values within a circle of radius r_s around P. As Graftieaux *et al.* [8] have shown, these quantities are relatively insensitive to discretization and work well even with a small number of integration points. However, it is crucial to choose an integration radius that is smaller than the size of the vortex in order to accurately capture its shape with Γ_2. Therefore, integration radii that are a few times larger than the characteristic size of the mesh elements are used to fulfill this criterion. To save computation time and memory and to focus on the detection on the TLV, the detection domain is restricted to the region near the blade tip.

These functions are robust to small-scale turbulence and can handle large data sets efficiently. They focus on the topology of the velocity field rather than its amplitude and are

therefore suitable for detecting large-scale eddies in turbulent flows.

In order to track the trajectory and shape of the vortex, several planes must be defined along the vortex path. For optimal detection and tracking, these planes must be perpendicular to the vortex trajectory, for a better circularity of the vortex section. As shown in Figure 7, the strategy is as follows:

1. For each position along the vortex trajectory, N candidate cutting planes are generated:
   (a) Generate a cutting plane centered on the estimated vortex center O_j with a normal vector $\mathbf{n}_j$.
   (b) Calculate the average direction of the vortex using the velocity vectors within the vortex shape detected by the Γ_2 sensor:

$$\mathbf{n}_j = \frac{\iint_{|\Gamma_2(P)|>2/\pi} \mathbf{U}_P \, \mathrm{d}S}{\left\| \iint_{|\Gamma_2(P)|>2/\pi} \mathbf{U}_P \, \mathrm{d}S \right\|} \tag{2}$$

   (c) Update the normal vector for the next cutting plane.
2. Among the N cutting planes computed, select the best plane i as the one that maximizes the sensor Γ_1.
3. Determine the position of the next plane using the projection method, where the center of the new plane is:

$$O_{i+1} = O_i + \ell \mathbf{n}_i \tag{3}$$

   Where ℓ is the distance increment, and O_i and $\mathbf{n}_i$ are the vortex center and the orientation of the current best detected plane.

One must provide a first cut that contains the vortex as an initialization. The process is repeated until the trajectory exceeds the detection range or the quality of the vortex detection decreases below $|\Gamma_1| = 0.85$.

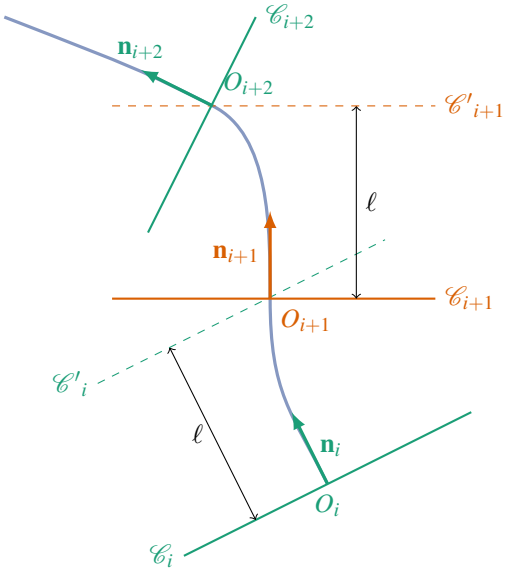

Figure 7: Strategy to build the succession of cutting planes. $\mathscr{C}_i$ denotes the ith analysis cut of origin O_i and of normal $\mathbf{n}_i$. The intermediate cut $\mathscr{C}'_i$ of origin $O_i + \ell \mathbf{n}_i$ and parallel to $\mathscr{C}_i$ is used to find the location O_{i+1} and the local direction $\mathbf{n}_{i+1}$ of the vortex core. Therefore the cut $\mathscr{C}_{i+1}$ is defined, and the process can continue.

As mentioned previously, the Γ_2 criterion can strictly only be applied for incompressible flows. However the criterion on Γ_1 does not rely on this hypothesis and can still be used to find the center of a vortex. Here we propose to substitute the criterion $|\Gamma_2| > 2/\pi$ as follows:

1. Generate a cutting plane centered on the detected vortex center O_j with a normal vector $\mathbf{n}_j$.
2. Compute the values of Γ_1 and find the location $\tilde{O}_j$ of its maximum absolute value.
3. Normalize any classic Galilean invariant by its maximum at the vortex center. For example, let us define the normalized sensor based on the Q-Criterion: $Q_n = Q/Q(\tilde{O}_j)$.
4. Calculate the average vortex direction based on the velocity vectors within the vortex core, defined as the region where the normalized invariant exceeds a certain threshold, e.g. $Q_n > 0.3$.

This procedure extracts the center and the core of the vortex, plane by plane. One can notice that, if the maximum value of the Galilean invariant at the vortex center is the same for each plane, then this procedure is similar to an iso-surface of the considered Galilean invariant.

4 Application of the method to the ECL5 simulations

The tip leakage flow of the ECL5 at nominal speed is highly turbulent. In order to apply the method developed, a filtered flow using Dynamic Mode Decomposition [25] is considered. The DMD offers the opportunity to build up a reduced order model of the flow, by choosing a reduced number of modes for the superposition.

The dataset considered contains 400 instantaneous 3D solutions of the rotor domain. Sampling was performed at 24 kHz (30 times the frequency of interest at 750 Hz) for 3 full rotations of the fan (12 periods of the phenomenon of interest). Therefore, the spectral resolution is $\Delta f \sim 60$ Hz. The DMD is performed using Antares, a python data processing library developed by CERFACS. The filtered flow is obtained by superposing the mean flow and modes near the frequency of interest, taking the spectral resolution into account. In this case, the mean flow and two modes are superposed, around 750 Hz.

Mean flow

First and foremost, the vortex detection is performed on the mean flow. The use of the method seems to indicate that it is more resilient if it is performed from downstream to upstream. The vortex detected by the method is represented in Figure 8a. The reference value of the Q-Criterion used by the method is shown in Figure 8b The evolution of the Γ_1 sensor at the detected vortex center is displayed in Figure 8c. The origin of the tip leakage vortex is located 4% axial chord downstream the leading edge at 99.5% of the rotor span. It can be noticed that the vortex detected is surrounded by supersonic regions (represented in gray) near the leading edge of the blade. Also the reference value of the Q-Criterion is strictly decreasing and drops by four orders of magnitude from the leading edge to the trailing edge. The values of the Γ_1 sensor remain close to the suggested threshold.

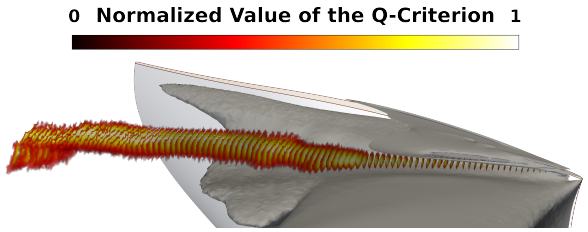

(a) Shape of the reconstructed vortex

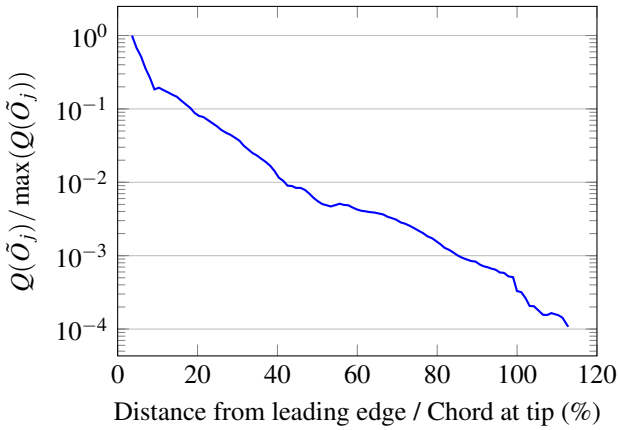

(b) Evolution of the reference value of the Q-Criterion along the vortex centerline

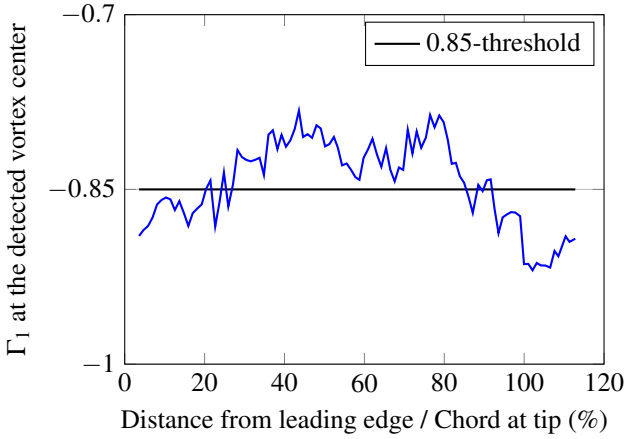

(c) Value of the Γ_1 sensor along the detected center of the vortex

Figure 8: Results of the vortex tracking algorithm applied to the mean flow. (a) Reconstructed vortex using the described method, colored by the normalized value of the Q-Criterion. The supersonic pocket is represented in gray. (b) Evolution of the reference value of the Q-criterion used to extract the core of the vortex for each analysis plane. (c) Evolution of the Γ_1 sensor at the vortex center. The sensor remains around the 0.85-threshold suggested by Graftieaux.

Comparison with the experiment

Figure 9 presents the ensemble-averaged wall static pressure distribution over the casing from the experimental measurements [26], as well as the vortex centerline obtained from the time-averaged LES. The location of the tip leakage vortex can be estimated using the pressure drop from the experimental ensemble-average. The origin of the reconstructed TLV from time-averaged LES appears to be 10% axial chord upstream

of the experimental pressure drop. This offset progressively reduces downstream. There is a good agreement between the TLV location and the pressure drop from 40% to 80% axial chord.

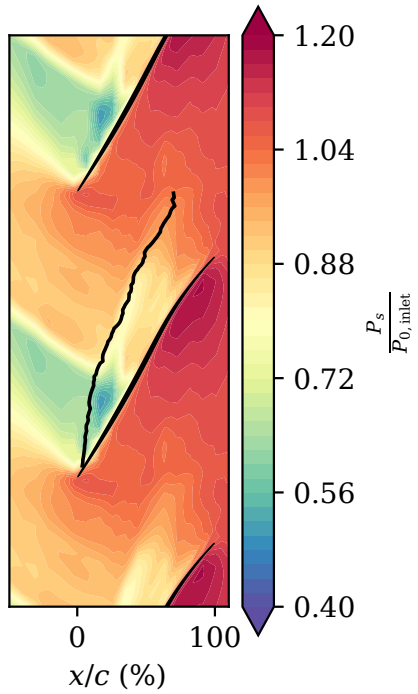

Figure 9: Experimental ensemble-averaged casing wall static pressure distribution and mean flow vortex centerline obtained from the LES.

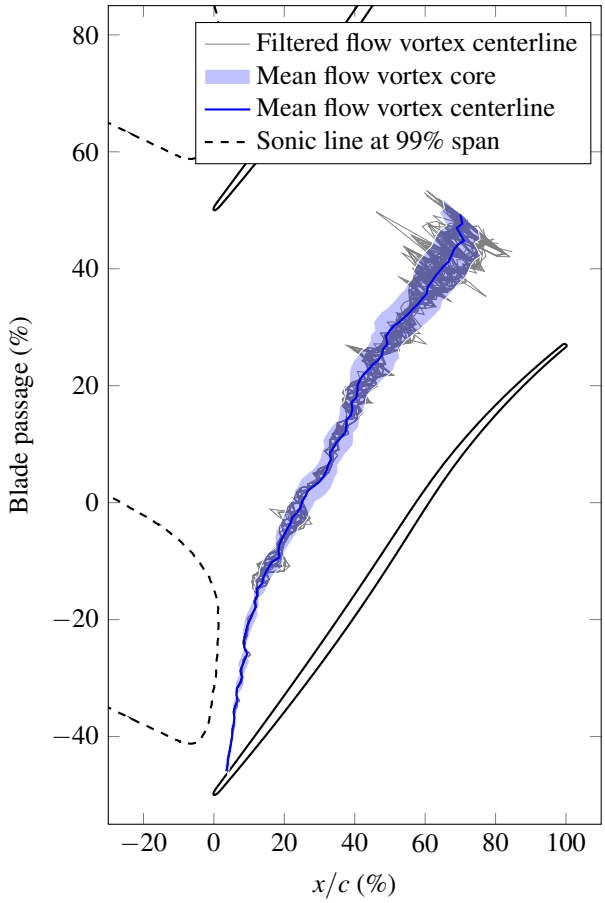

Figure 10: Blade to blade view at 99% of the span of the reconstructed vortex shapes obtained by the vortex tracking algorithm.

Filtered flow around the frequency of interest

The analysis now focuses on the filtered flow around the frequency of interest (750 Hz). The origins and orientations of the planes computed from the mean flow analysis are a good first guess in order to apply the algorithm on the filtered dataset. Thus, for each snapshot of the reconstructed flow, for each plane, the vortex tracking is applied using the mean flow parameters as a first guess. The usual procedure is still applied in order to slightly adjust the orientation of the cutting planes and the deviation of the vortex centerline. Figure 10 sums up the entire results of the vortex tracking algorithm over the filtered data. The figure is a blade to blade view of the vortex centerline of the mean flow ——, as well as the vortex centerline of one hundred consecutive snapshots of the filtered flow ——. The core of the mean flow vortex is also represented ▬, as well as the upstream sonic line at 99% of span - - -. Near the leading edge and up to 10% axial chord downstream, all vortex centerlines from the filtered flow stand still. Then, around $x/c = 0.2$ the vortex centerlines of the filtered flow spread but remain inside the core of the mean flow vortex. The variability of the vortex centerline seems to increase just downstream the shock-wave.

In this present case, non-negligible oscillations are identified. The Strouhal number associated with the oscillation (based on the chord length and the relative upstream velocity) is $\mathrm{St} = 0.22$. A wandering vortex phenomenon could exist regarding the range of Strouhal number [27, 28], and explain the observed oscillations. However, the vortex remains still near the leading edge, with no azimuthal displacement. The amplitude of oscillations increases with the axial position after the shock-wave. The observed phenomenon could be the response of the vortex while being exited to this frequency.

The mechanisms behind the low frequency phenomenon remains under investigation.

5 Conclusions

In the present study, a methodology was introduced to track a vortex in a complex configuration. This method is based on the Γ_1 and Γ_2 sensors introduced by Graftieaux *et al.*, and was extended to compressible flows using usual Galilean invariants, such as the Q-Criterion. This method has been developed in order to track the tip-leakage vortex in LES of the ECL5 fan/OGV stage at a transonic regime. This vortex tracking algorithm has been applied on both the mean flow and a filtered flow reconstructed from a dynamic mode decomposition. The results obtained on the mean flow have shown

that the vortex was surrounded by supersonic regions near the leading edge. The algorithm used a range of reference values of the Q-Criterion that extends over four orders of magnitude. The trajectory of the mean flow vortex centerline seems coherent with the experimental wall static pressure distribution on the casing. Using the mean flow results, the method has been applied over hundreds of frequency filtered instantaneous flows. While the vortex centerline remains stationary close to the leading edge, the variability of the vortex trajectories suddenly increases just downstream the shockwave. This variability of the vortex centerline is of the order of the mean vortex core radius.

The next step is to apply this method to operating points near the stability limit.

Acknowledgements

The results presented in this paper rely on the contributions of a large research group, and the authors gratefully acknowledge their excellent collaboration and support over the past five years. The authors thank the whole turbomachinery experimental LMFA team, especially Alexandra Schneider for the experimental data post-processing and analysis. The authors recall that the development of the fan was conducted within the thesis of Valdo Pages and supervised by Stephane Aubert, Pascal Ferrand, and Pierre Duquesne from LMFA, as well as Laurent Blanc from LTDS. The final design was developed in close collaboration with Safran Aircraft Engines. We are grateful for the continuous collaboration and financial support of SAFRAN Aircraft Engines since the beginning of this project and specifically for the present measurement campaign, for which the test module MARLYSA was provided by SAFRAN. The authors particularly thank Jean Al-Am for his turbomachinery LES expertise, and the advice given the past four years.

The present work was supported by CIRT (Consortium Industrie-Recheche en Turbomachines) in the frame of the *Sonos* project.

The computational resources for the LES were provided by GENCI (IRENE, project number A0142A05039). This work was granted access to the HPC resources of PMCS2I (Pôle de Modélisation et de Calcul en Sciences de l'Ingénieur et de l'Information) of École Centrale de Lyon, Écully, France. Post-processing were performed using the python library Antares (release 1.19.0).

References

[1] J. Boudet, A. Cahuzac, P. Kausche, and M. C. Jacob. "Zonal Large-Eddy Simulation of a Fan Tip-Clearance Flow, With Evidence of Vortex Wandering". In: *Journal of Turbomachinery* 137.61001 (June 1, 2015). ISSN: 0889-504X. DOI: 10.1115/1.4028668.

[2] V. Pagès, P. Duquesne, S. Aubert, L. Blanc, P. Ferrand, X. Ottavy, and C. Brandstetter. "UHBR Open-Test-Case Fan ECL5/CATANA". In: *IJTPP* 7.2 (May 31, 2022), p. 17. ISSN: 2504-186X. DOI: 10.3390/ijtpp7020017.

[3] C. Brandstetter, V. Pages, P. Duquesne, X. Ottavy, P. Ferrand, S. Aubert, and L. Blanc. "UHBR Open-test-case fan ECL5/Catana, Part 1: Geometry and aerodynamic performance". In: *European Conference on Turbomachinery Fluid Dynamics and Thermodynamics*. European Conference on Turbomachinery Fluid Dynamics and Thermodynamics. Virtual Conference: European Turbomachinery Society, 2021. DOI: 10.29008/ETC2021-626.

[4] V. Pagès, P. Duquesne, X. Ottavy, P. Ferrand, S. Aubert, L. Blanc, and C. Brandstetter. "UHBR Open-test-case fan ECL5/Catana, Part 2: Mechanical and aeroelastic stability analysis". In: *European Conference on Turbomachinery Fluid Dynamics and Thermodynamics*. European Conference on Turbomachinery Fluid Dynamics and Thermodynamics. Virtual Conference: European Turbomachinery Society, 2021. DOI: 10.29008/ETC2021-625.

[5] J. C. R. Hunt, A. A. Wray, and P. Moin. "Eddies, streams, and convergence zones in turbulent flows". In: (Dec. 1, 1988). NTRS Author Affiliations: Cambridge Univ. (England)., NASA Ames Research Center, Stanford Univ. NTRS Document ID: 19890015184 NTRS Research Center: Legacy CDMS (CDMS).

[6] M. S. Chong, A. E. Perry, and B. J. Cantwell. "A general classification of three-dimensional flow fields". In: *Physics of Fluids A: Fluid Dynamics* 2.5 (May 1, 1990), pp. 765–777. ISSN: 0899-8213. DOI: 10.1063/1.857730.

[7] J. Jeong and F. Hussain. "On the identification of a vortex". In: *Journal of Fluid Mechanics* 285 (Feb. 1995), pp. 69–94. ISSN: 1469-7645, 0022-1120. DOI: 10.1017/S0022112095000462.

[8] L. Graftieaux, M. Michard, and N. Grosjean. "Combining PIV, POD and Vortex Identification Algorithms for the Study of Unsteady Turbulent Swirling Flows". In: *Measurement Science and Technology* 12.9 (Sept. 2001), pp. 1422–1429. ISSN: 0957-0233, 1361-6501. DOI: 10.1088/0957-0233/12/9/307.

[9] C. E. Simpson, H. Babinsky, J. K. Harvey, and S. Corkery. "Detecting vortices within unsteady flows when using single-shot PIV". In: *Exp Fluids* 59.8 (July 7, 2018), p. 125. ISSN: 1432-1114. DOI: 10.1007/s00348-018-2575-3.

[10] M. Coletta, F. D. Gregorio, A. Visingardi, and G. Iuso. "PIV data: Vortex Detection and Characterization". In: *International Symposium on Particle Image Velocimetry* (2019).

[11] C. Brandstetter, A. P. Schneider, A.-L. Fiquet, B. Paoletti, and X. Ottavy. "Experiments on Structurally Mistuned UHBR Open-Test-Case Fan ECL5/CATANA". In: ASME Turbo Expo 2024: Turbomachinery Technical Conference and Exposition. American Society of Mechanical Engineers Digital Collection, Aug. 28, 2024. DOI: 10.1115/GT2024-129163.

[12] M. M. Rai and N. K. Madavan. "Multi-Airfoil Navier–Stokes Simulations of Turbine Rotor–Stator Interaction". In: *Journal of Turbomachinery* 112.3 (July 1, 1990), pp. 377–384. ISSN: 0889-504X, 1528-8900. DOI: 10.1115/1.2927670.

[13] T. Schonfeld and M. Rudgyard. "Steady and Unsteady Flow Simulations Using the Hybrid Flow Solver AVBP". In: *AIAA Journal* 37.11 (Nov. 1999). Publisher: American Institute of Aeronautics and Astronautics, pp. 1378–1385. ISSN: 0001-1452. DOI: 10.2514/2.636.

[14] S. Moreau. "Turbomachinery-related aeroacoustic modelling and simulation". en. In: *17th International Conference on Fluid Flow Technologies*. 2018.

[15] J. Al-Am, A. Giauque, V. Clair, J. Boudet, and F. Gea-Aguilera. "Direct-Noise of an Ultrahigh-Bypass-Ratio Turbofan: Periodic-Sector vs Full-Annulus Large-Eddy Simulations". In: *AIAA Journal* (May 8, 2024). Publisher: American Institute of Aeronautics and Astronautics (AIAA), pp. 1–15. ISSN: 0001-1452, 1533-385X. DOI: 10.2514/1.j063596.

[16] G. Wang, F. Duchaine, D. Papadogiannis, I. Duran, S. Moreau, and L. Y. M. Gicquel. "An overset grid method for large eddy simulation of turbomachinery stages". In: *Journal of Computational Physics* 274 (Oct. 1, 2014), pp. 333–355. ISSN: 0021-9991. DOI: 10.1016/j.jcp.2014.06.006.

[17] J. de Laborderie, F. Duchaine, L. Gicquel, O. Vermorel, G. Wang, and S. Moreau. "Numerical analysis of a high-order unstructured overset grid method for compressible LES of turbomachinery". In: *Journal of Computational Physics* 363 (June 15, 2018), pp. 371–398. ISSN: 0021-9991. DOI: 10.1016/j.jcp.2018.02.045.

[18] F. Duchaine, S. Jauré, D. Poitou, E. Quémerais, G. Staffelbach, T. Morel, and L. Gicquel. "Analysis of high performance conjugate heat transfer with the OpenPALM coupler". en. In: *Comput. Sci. Discov.* 8.1 (July 2015). Publisher: IOP Publishing, p. 015003. ISSN: 1749-4699. DOI: 10.1088/1749-4699/8/1/015003.

[19] O. Colin and M. Rudgyard. "Development of High-Order Taylor–Galerkin Schemes for LES". en. In: *Journal of Computational Physics* 162.2 (Aug. 2000), pp. 338–371. ISSN: 00219991. DOI: 10.1006/jcph.2000.6538.

[20] F. Nicoud, H. B. Toda, O. Cabrit, S. Bose, and J. Lee. "Using singular values to build a subgrid-scale model for large eddy simulations". In: *Physics of Fluids* 23.8 (Aug. 2011), p. 085106. ISSN: 1070-6631. DOI: 10.1063/1.3623274.

[21] A. W. Cook and W. H. Cabot. "Hyperviscosity for shock-turbulence interactions". In: *Journal of Computational Physics* 203.2 (Mar. 2005), pp. 379–385. ISSN: 0021-9991. DOI: 10.1016/j.jcp.2004.09.011.

[22] T. J. Poinsot and S. K. Lelef. "Boundary conditions for direct simulations of compressible viscous flows". In: *Journal of Computational Physics* 101.1 (July 1992), pp. 104–129. ISSN: 0021-9991. DOI: 10.1016/0021-9991(92)90046-2.

[23] P. Schmitt, T. Poinsot, B. Schuermans, and K. P. Geigle. "Large-eddy simulation and experimental study of heat transfer, nitric oxide emissions and combustion instability in a swirled turbulent high-pressure burner". en. In: *Journal of Fluid Mechanics* 570 (Jan. 2007). Publisher: Cambridge University Press, pp. 17–46. ISSN: 0022-1120, 1469-7645. DOI: 10.1017/S0022112006003156.

[24] F. Jaegle, O. Cabrit, S. Mendez, and T. Poinsot. "Implementation Methods of Wall Functions in Cell-vertex Numerical Solvers". en. In: *Flow Turbulence Combust* 85.2 (Sept. 2010), pp. 245–272. ISSN: 1573-1987. DOI: 10.1007/s10494-010-9276-1.

[25] P. Schmid. "Dynamic mode decomposition of numerical and experimental data". In: *Journal of Fluid Mechanics* 25 (July 1, 2010), pp. 249–259. ISSN: 0022-1120. DOI: 10.1017/S0022112010001217.

[26] A. P. Schneider. "Aerodynamic and aeroelastic investigation of a composite fan for ultra-high-bypass-ratio aircraft engines". These de doctorat. Ecully, Ecole centrale de Lyon, May 22, 2024.

[27] W. J. Devenport, M. C. Rife, S. I. Liapis, and G. J. Follin. "The structure and development of a wing-tip vortex". In: *J. Fluid Mech.* 312 (Apr. 10, 1996), pp. 67–106. ISSN: 0022-1120, 1469-7645. DOI: 10.1017/S0022112096001929.

[28] A. M. Edstrand, T. B. Davis, P. J. Schmid, K. Taira, and L. N. Cattafesta. "On the mechanism of trailing vortex wandering". In: *J. Fluid Mech.* 801 (Aug. 25, 2016), R1. ISSN: 0022-1120, 1469-7645. DOI: 10.1017/jfm.2016.440.